ACS Catalysis

pubs.acs.org/acscatalysis

Research Article

Interplay between CO Disproportionation and Oxidation: On the Origin of the CO Reaction Onset on Atomic Layer Deposition-Grown Pt/ZrO_2 Model Catalysts

Verena Pramhaas, Matteo Roiaz, Noemi Bosio, Manuel Corva, Christoph Rameshan, Erik Vesselli, Henrik Grönbeck, and Günther Rupprechter*

Cite This: *ACS Catal.* 2021, 11, 208−214

Read Online

ACCESS | Metrics & More | Article Recommendations | Supporting Information

ABSTRACT: Pt/ZrO_2 model catalysts were prepared by atomic layer deposition (ALD) and examined at mbar pressure by *operando* sum frequency generation (SFG) spectroscopy and near-ambient pressure X-ray photoelectron spectroscopy (NAP-XPS) combined with differentially pumped mass spectrometry (MS). ALD enables creating model systems ranging from Pt nanoparticles to bulk-like thin films. Polarization-dependent SFG of CO adsorption reveals both the adsorption configuration and the Pt particle morphology. By combining experimental data with *ab initio* density functional theory (DFT) calculations, we show that the CO reaction onset is determined by a delicate balance between CO disproportionation (Boudouard reaction) and oxidation. CO disproportionation occurs on low-coordinated Pt sites, but only at high CO coverages and when the remaining C atom is stabilized by a favorable coordination. Thus, under the current conditions, initial CO oxidation is found to be strongly influenced by the removal of carbon deposits formed through disproportionation mechanisms rather than being determined by the CO and oxygen inherent activity. Accordingly, at variance with the general expectation, rough Pt nanoparticles are seemingly less active than smoother Pt films. The applied approach enables bridging both the "materials and pressure gaps".

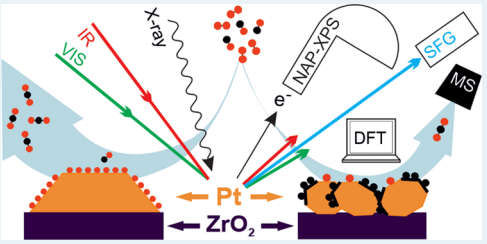

KEYWORDS: *Pt nanoparticles, catalysis, in situ spectroscopy, operando, SFG, NAP-XPS, DFT*

The adsorption and catalytic oxidation of CO on Pt are among the most frequently examined surface processes due to their environmental and industrial relevance. Pt exhibits superior catalytic properties for various applications, such as (preferential) CO oxidation for emission control or cleaning of hydrogen streams for fuel cells.[1−5] Despite efforts to replace expensive Pt by cheaper materials, its activity can typically not be matched. Thus, the focus is rather on reducing the Pt amount, e.g., by using Pt atoms, clusters, and small nanoparticles[6−13] (or alloys and core−shell structures[14,15]) on suitable support materials. It is, however, still challenging to obtain detailed knowledge about increasingly smaller nanoparticles, especially about their inherent activity and metal/support interaction.[16−21]

In recent years, significant advances have been made in model catalysis, enabling surface characterization at (near) atmospheric pressure, overcoming the "pressure gap",[22−31] but bridging the "materials gap" is evenly important. Previous single-crystal studies have provided fundamental insight, but they cannot fully mimic nanoparticles[25,32,33] (with support effects being apparently inaccessible), which is why more realistic model systems are required, such as oxide-supported nanoparticles/islands[11,16,25,34] or inverse systems.[35−37]

In this contribution, we present Pt/ZrO_2 model catalysts prepared by atomic layer deposition (ALD) that were examined at mbar pressures by *operando* sum frequency generation (SFG) spectroscopy and near-ambient pressure X-ray photoelectron spectroscopy (NAP-XPS), with simultaneous mass spectrometry (MS) product analysis, and complemented by density functional theory (DFT) calculations.

ALD has been widely used in industrial manufacturing,[38,39] especially for dielectrics and microelectronics, and is receiving increasing attention for (upscalable) catalyst preparation.[40] The current model catalysts consist of a zirconia film, ALD-grown (400 cycles) on a Si (100) wafer, and Pt deposits prepared by different numbers of ALD cycles (10−250; see transmission electron microscopy (TEM) images in Figure 1a and Figure S3). Whereas the zirconia ALD generated a uniform 42 nm-thick oxide support, using a few (10, 50) Pt cycles produced small Pt particles up to 8 nm in size (Figure 1a, right panel). Upon applying 125 or 250 deposition cycles, the Pt particles coalesced into islands, finally forming a homogeneous Pt film of uniform ∼10 nm thickness (Figure 1a,

Received: September 10, 2020
Revised: November 4, 2020
Published: December 17, 2020

https://dx.doi.org/10.1021/acscatal.0c03974
ACS Catal. 2021, 11, 208−214

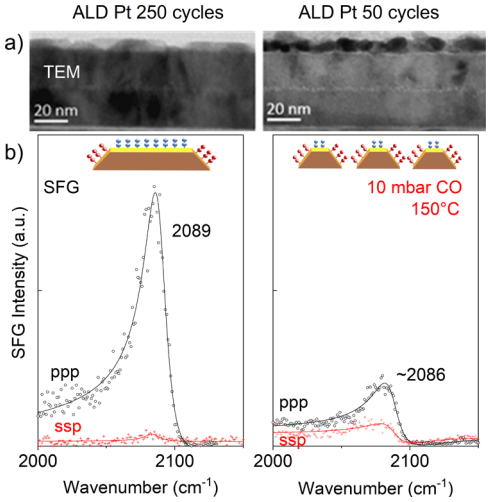

Figure 1. (a) Cross-sectional TEM micrographs of 250 cycle and 50 cycle Pt films. The 250 cycle film consists of large uniform and planar islands (~10 nm in thickness), whereas the 50 cycle film is made up of individual Pt particles (size of about 8 nm). (b) SFG spectra in two different polarization combinations (ppp and ssp) of adsorbed CO (10 mbar at 150 °C); the surface morphology of islands/particles (see models) can be assessed by comparing the ppp to ssp intensity (ppp (ssp) has a higher intensity if the C═O bond is parallel (tilted) to the macroscopic surface normal).

left panel). These nucleation and growth processes[41] allow for the preparation of different well-defined Pt/ZrO_2 model catalysts ranging from isolated Pt nanoparticles to bulk-like thin films. Herein, the 50 and 250 cycle samples are the most informative ones (other samples are described in the Supporting Information). The ALD approach to catalyst synthesis is not new,[42,43] but the combination with *operando* surface spectroscopy (SFG and NAP-XPS carried out in high-pressure cells with simultaneous MS gas-phase analysis) and DFT calculations provides a complementary picture.

The standard cleaning used for single crystals in ultrahigh vacuum (UHV), i.e., sputtering/annealing, could not be applied as it would have destroyed the ALD samples. Inspired by the (re-)activation of technological catalysts, all samples were thus cleaned from carbonaceous residues by heating in 10 mbar O_2 to 400 °C and in 20 mbar CO/O_2 (1:1) to 300 °C.

The Pt morphology was then addressed by polarization-dependent SFG of CO adsorption (10 mbar CO at 150 °C; Figure 1b; see the Supporting Information for SFG theory and fit values). The spectra show the on-top CO resonance region, as no other binding geometries were observed. Two polarization combinations were employed: ppp (has its maximum intensity for C═O bonds parallel to the macroscopic surface normal; black in Figure 1b) and ssp (has its maximum intensity for C═O bonds inclined with respect to the macroscopic surface normal, i.e., around 30−40° depending on molecular polarizability; red in Figure 1b).[44,45] Due to the angular dependence, the resulting intensity ratio I_{ppp}/I_{ssp} for CO is expected to decrease with increasing bond inclination of the molecules.[46,47] Because the Pt film of the 250 cycle sample consisted of planar islands with a uniform height of about 10 nm, adsorbed CO was mostly perpendicular to the ZrO_2/Si(100) surface so that the CO peak intensity was high in ppp and very low in ssp (ratio of 17.4). In light of our previous study of CO/Pt(111),[47] assuming an identical optical interface model, this would correspond to an average CO tilt angle of ~5° (relative to the macroscopic surface normal), although this value is just meant to show a trend. In contrast, the 50 ALD cycle Pt film consisted of small particles (about 8 nm) with multiple facets, many of which are no longer parallel to the substrate. On these inclined facets, CO still adsorbs

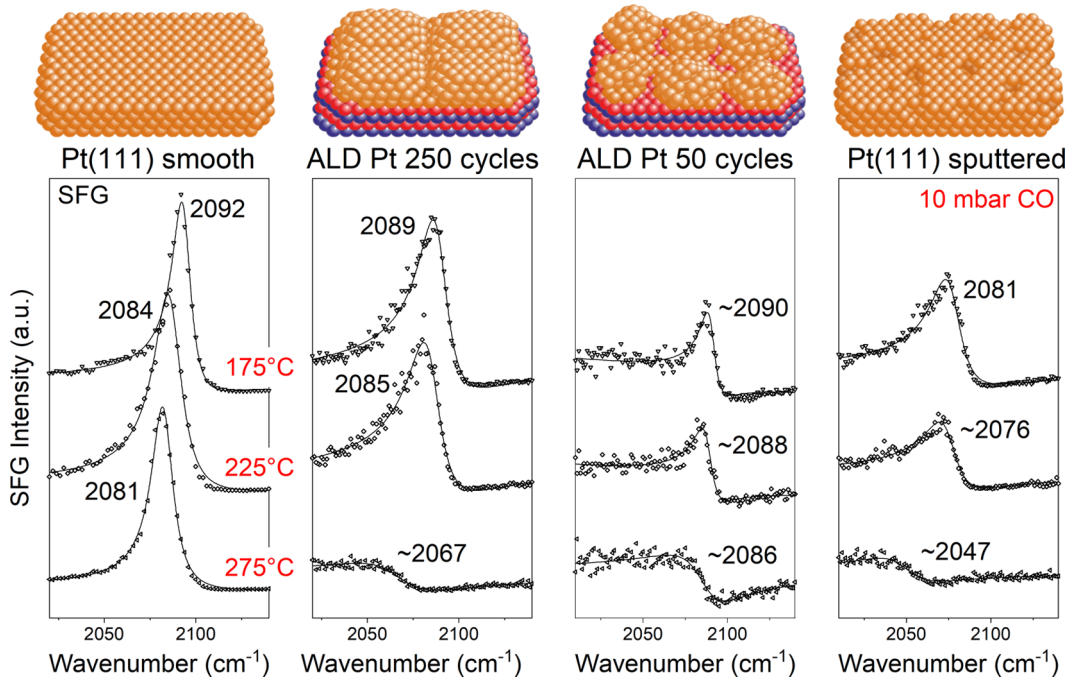

Figure 2. SFG spectra (ppp polarization) displaying on-top CO on different Pt surfaces, acquired in 10 mbar CO at the indicated temperatures. The surface roughness increases from left to right, as indicated by the decreasing intensity and redshift of resonance positions. The indicated values were obtained from data fits (solid lines). For rough surfaces, spectra at 275 °C showed a diminishing on-top CO, which was irreversible upon cooldown (Figure S10). This cannot be explained by a decrease in CO coverage, as for Pt(111), the spectrum remained almost unchanged.

https://dx.doi.org/10.1021/acscatal.0c03974
ACS Catal. 2021, 11, 208−214

perpendicularly, but the CO bonds are inclined with respect to the macroscopic surface normal. Accordingly, the SFG intensity is lower in ppp, resulting in a much lower I_{ppp}/I_{ssp} ratio of 2.3. Following the same assumptions as above, the average CO tilt angle would be ~40° (note that this again is just to show the trend). This rough estimate agrees with the facet inclination and ratio from TEM images.

Apart from the intensity, the peak position and peak symmetry/asymmetry are noteworthy. The peak position depends on the coordination of the Pt adsorption site and the CO surface coverage (inducing chemical and dipole−dipole interactions).[27,48,49] As the coverage should be (nearly) the same under identical pressure and temperature conditions, the 3 cm^{-1} difference points to slightly rougher surfaces for the nanoparticle sample. The (a)symmetry of an SFG signal depends on the amplitudes A_r or A_{nr} and phase difference ϕ between resonant (adsorbed CO) and nonresonant signal contributions[50−52] (see the Supporting Information). The nonresonant background A_{nr} may originate from Pt surface defects (changing the electron localization at the surface) and electronic contributions of the ZrO_2/Si(100) substrate. Comparing the spectra of the 250 and 50 cycle samples, the intensities of the resonant and nonresonant contributions are much more similar in the case of the particulate film (smaller particle size, more defects, and more metal/oxide interface), while the resonance phase relative to the nonresonant background, as obtained by means of the quantitative deconvolution of the data, is found to be similar for both CO-Pt systems. This leads to a more asymmetric line shape for the 50 cycle Pt, directly reflecting its surface morphology.

In order to further characterize the ALD-prepared model catalysts, they were compared to Pt single crystals at different temperatures. Figure 2 shows the SFG ppp spectra of smooth (UHV annealed to 800 °C) Pt(111), 250 and 50 ALD cycle Pt/ZrO_2, and sputtered Pt(111) in 10 mbar CO. Respective fitting values are given in the Supporting Information (our system has a spectral accuracy of 2 cm^{-1}). At 175 °C, the characteristic on-top CO on Pt(111) was observed at 2092 cm^{-1}, matching the saturation coverage.[49,53] The 250 cycle sample exhibited a continuous Pt surface (Figure 1 and Figures S2 and S3), but was still rougher than the annealed Pt(111), as indicated by the redshifted wavenumber (2089 cm^{-1}) and increased peak asymmetry. Adsorbed CO on the 50 cycle Pt/ZrO_2 sample, consisting of 8 nm (connected) particles, exhibited a similar wavenumber, indicating identical coordination, but lower intensity and higher asymmetry due to the inclined facets. The higher number of low-coordinated (step/kink) sites[54,55] on the ALD samples was confirmed by comparison with the CO spectra of sputtered Pt(111) (2081 cm^{-1}) and Pt(110) (2075 cm^{-1}) (Figure S9), showing even lower wavenumbers.[53,56] Apparently, the ALD Pt catalysts exhibit roughness intermediate between the annealed and sputtered Pt(111).

Now, turning to the CO adsorption at higher temperatures (225/275 °C), the decreased CO coverage induced a redshift.[24,48,49,53] For Pt(111), the on-top CO signal redshifted, but the intensity was similar to that at 175 °C. Analogously, the CO signals of the ALD samples and sputtered Pt(111) exhibited small redshifts at 225 °C (and a minor intensity loss). However, at 275 °C, the rougher surfaces showed a pronounced intensity loss, peak shift, and phase alteration. Previously, a similar observation on polycrystalline Pt foil[57] was explained by CO desorption, but CO is more strongly bonded to steps/defects than terraces.[58,59] Furthermore, the spectral changes were irreversible upon cooldown in CO (see Figure S10) and ϕ changed significantly, ruling out simple adsorption/desorption and rather suggesting a permanent modification/blocking of the adsorption sites. It has been reported that stepped Pt surfaces or small Pt particles/clusters may cause CO dissociation, forming a carbon overlayer,[60] in line with the current observation. Indeed, the CO spectrum of the 250 cycle Pt at 10 mbar/225 °C agrees quite well with the reported values of Pt(557) at 30 mbar/250 °C, which showed CO dissociation at 275 °C. The dissociation hypothesis is supported by the fact that adding O_2 to CO and heating reversed the spectral change by reoxidizing carbon to CO_2 (Figure S11). Nevertheless, CO dissociation on Pt has been controversially discussed for a long time.

This motivated the DFT calculations of CO dissociation on smooth and rough Pt surfaces (Figure 3). CO dissociation on

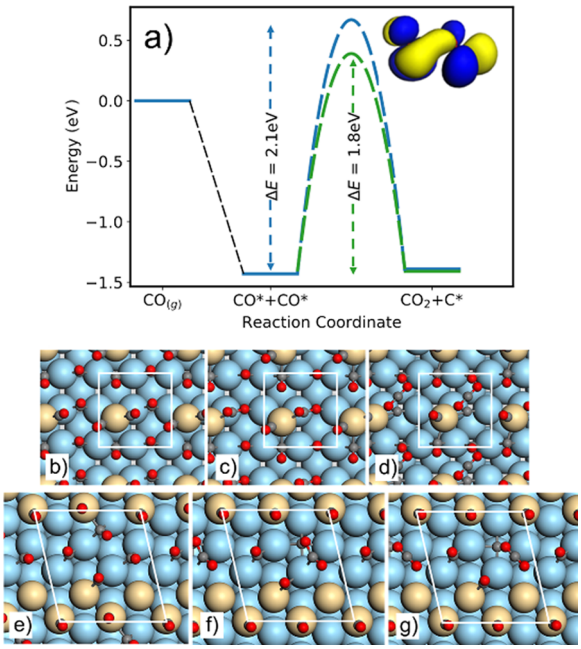

Figure 3. (a) Potential energy diagram for CO disproportionation over an adatom on Pt(100) (green) and Pt(410) (blue). The dissociation is evaluated at the CO coverage given by a thermodynamic analysis, and the zero level is the saturation coverage minus one CO molecule and one CO molecule in the gas phase. The inset shows the HOMO orbital for $(CO−CO)^{2−}$. Panels (b)−(d) and (e)−(g) show the initial, transition, and final states for dissociation at an adatom on Pt(100) and Pt(410), respectively. Atomic color code: C (dark gray), O (red), Pt adatom or top layer (beige), and Pt (light blue).

Pt(111) and Pt(211) is strongly endothermic and barriers >3 eV have been reported in the low coverage limit,[61] making this process improbable. For a more facile dissociation, the adsorbed state of CO should be destabilized, whereas the final state needs to be stabilized. A destabilization of the adsorbed state is achieved by increasing the coverage (gas pressure), whereas the final state is stabilized by CO_2 formation. In particular, direct CO_2 formation according to the Boudouard reaction (CO* + CO* → CO_2 + C*) hinders the backward C−O association reaction. Similar contributions (local coverage and final state) to favoring the Boudouard reaction have been reported for PtSn[61] and Cu.[62,63] For

https://dx.doi.org/10.1021/acscatal.0c03974
ACS Catal. 2021, 11, 208−214

efficient CO−CO coupling and reaction, the C weight of the $2\pi^*$ orbital on one reacting molecule should overlap with the O weight on the other molecule. This may be accomplished on stepped and kinked surfaces, so we considered two model structures: a Pt adatom coordinated with two CO molecules on Pt(100) and Pt(410). The barriers were evaluated at coverages obtained from a thermodynamic analysis (Figures S14 and S15). The barriers for the reactions are 1.8 and 2.1 eV for dissociation at the adatom and Pt(410), respectively. For the reaction at the adatom (Figure 3b−d), one of the CO molecules on the Pt adatom is reacting with a CO on the (100) facet. The transition state is a bent O−C−O structure (Figure 3c), whereas the final state (Figure 3d) is gas-phase CO_2 and the remaining carbon atom is in a highly coordinated position. A fourfold coordinated C on Pt(100) is (per carbon atom) as stable as graphite, thus stabilizing the final state.[64] The reaction path on Pt(410) is different as both reacting CO molecules are below the step (Figure 3e−g). The $2\pi^*-2\pi^*$ match is, in this case, enabled by an initial bending of the CO close to the step, and the final state again has a fourfold coordinated C atom. Accordingly, on the rougher Pt surfaces, CO dissociation is facilitated by a barrier that is lower than 1 eV as compared to the smooth surfaces.

Turning to CO oxidation on the Pt/ZrO_2 model catalysts, Figure 4a,b shows the SFG ppp spectra acquired in a reaction mixture of 10 mbar CO and 20 mbar O_2 from 150 to 500 °C. At 150 °C, the Pt particles were on-top CO-covered (poisoned) and thus inactive, with 2091 cm^{-1} indicating high-coordination sites for the 250 cycle sample. The 50 cycle sample showed a 10 cm^{-1} redshift, indicating lower coordination/higher roughness, with lower intensity and more asymmetry, due to the nanoparticle morphology. Upon temperature increase, the peak of adsorbed CO decreased and redshifted (due to decreasing CO coverage) and finally disappeared when the Pt surfaces were fully oxygen-covered and thus active: at 400 °C for the Pt thin film, but at 450 °C for the Pt nanoparticles. The temperature-dependent shifts were 2091−2080 cm^{-1} for the smoother Pt film and 2081−2074 cm^{-1} for the rougher Pt nanoparticles, the latter wavenumbers indicating stronger bonding on the rougher surfaces. The ignition temperatures were corroborated by the simultaneously acquired CO_2-MS traces in Figure 4c,d and are in accordance with values reported in the literature[31,65] (note that MS measurements without simultaneous SFG, "laser-off", ruled out any laser-induced effects; Figure S16). As long as adsorbed CO is present, the oxidation reaction is largely inhibited, as the Pt surface can only be in a single stable state, either CO-poisoned (inactive) or O-covered (active).[66] Accordingly, both SFG and MS indicated that about 50 °C higher temperature was required for ignition on the rougher (50 cycle) Pt nanoparticles. This is unexpected, because rougher Pt surfaces are generally considered to be more active in CO oxidation,[9,66] as their low-coordinated sites (steps, kinks, and edges) bind both oxygen and CO stronger than terraces. The O-covered active state can be more easily established on rougher surfaces (indicated by the lower ignition temperature and higher CO tolerance) despite the higher CO oxidation barriers[67] (according to the Brønsted−Evans−Polanyi relation[68]). However, in the current case, the inherent activity is not the only important factor, as shown in the following.

To further examine the reaction onset, NAP-XPS was applied as the second *operando* technique (which again rules

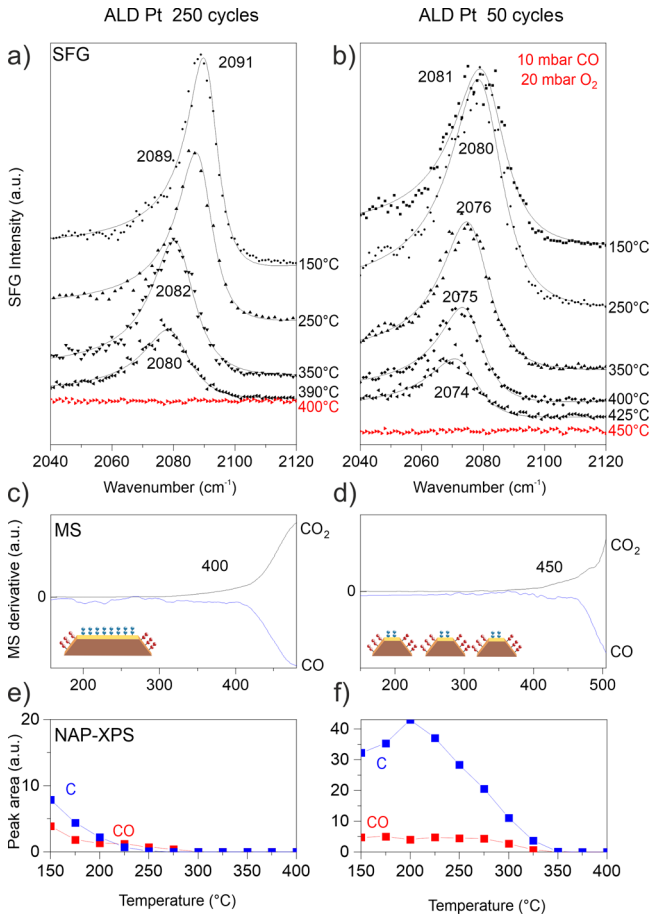

Figure 4. (a, b) SFG spectra (ppp polarization) acquired in 10 mbar CO + 20 mbar O_2 (batch mode) for the 250 and 50 cycle ALD Pt samples. The spectra redshift at higher temperatures due to reduced CO coverage until the surfaces fully switch to oxygen coverage. (c, d) Derivatives of the mass spectrometry data of CO and CO_2. For the rougher 50 cycle film, both the disappearance of CO in SFG and the onset of CO_2 production are shifted to higher temperature. (e, f) Temperature-dependent evolution of adsorbed CO and carbon deduced from C 1s NAP-XPS (1 mbar CO, 2 mbar O_2; flow mode).

out laser-induced effects). Due to technical limitations, the pressure was limited to 1 mbar CO and 2 mbar O_2. The C 1s spectra acquired during CO oxidation (Figure S17) detected graphitic carbon (284.7 eV),[69] adsorbed CO (286.2 eV),[59,70] a weak shoulder (around 288 eV; likely carbonate on zirconia), and gas-phase CO (~291 eV). Figure 4e,f displays the fitted peak areas vs (increasing) temperature for adsorbed CO and carbon. In analogy to SFG, for smoother (250 cycles) Pt films, CO fully disappears at a temperature 50 °C lower than for rougher (50 cycles) Pt nanoparticles (the absolute temperatures are lower due to the 10-fold lower pressure).

However, NAP-XPS showed that much more carbon was present during the reaction on the 50 cycle (rough) Pt nanoparticles, which even increased during the first two temperature steps, clearly indicating CO disproportionation (Figure 4f). Atomic carbon apparently poisons the (low-coordinated) active sites for oxygen activation until it is removed by oxygen at higher temperatures. This effect explains the higher reaction onset temperature of the Pt nanoparticles despite their presumably more active surface. In contrast, the smoother 250 cycle Pt film was much less affected by C poisoning, yielding a lower reaction onset temperature. After

https://dx.doi.org/10.1021/acscatal.0c03974
ACS Catal. 2021, 11, 208−214

ignition, both Pt surfaces were O-covered and showed the expected hysteresis upon lowering the temperature (Figure S19). CO readsorbed at a comparably lower temperature paralleled by less coking (due to cooling in an oxygen-containing atmosphere). Throughout all experiments, the *operando* Pt 4f spectra revealed that Pt remained metallic (Figure S17).

In summary, combining the ALD model catalyst preparation, *operando* SFG/NAP-XPS/MS spectroscopy, and DFT calculations enabled us to build another bridge across the "materials and pressure gap". Few ALD Pt deposition cycles produced Pt nanoparticles with multiple inclined facets, whereas more deposition cycles (≥125) led to more uniform Pt films. The polarization-dependent SFG revealed the molecular orientation of CO (relative to the macroscopic surface normal) and thus both the morphology and roughness of different ALD-grown Pt model catalysts. Upon CO adsorption at mbar pressure around 275 °C, Pt(111) did not show CO disproportionation, whereas rougher Pt particles/films and sputtered Pt(111) did. According to the DFT calculations, direct CO dissociation is unfeasible even at stepped Pt surfaces. Dissociation instead occurs at high coverages via a disproportionation reaction at low-coordinated sites that structurally promote CO−CO coupling and stabilize the remaining C atom. The effect of surface roughness on the CO oxidation was monitored at mbar pressure and elevated temperature by correlating the *operando* SFG and NAP-XPS spectra with the MS reactivity data. Different from the general expectation, the reaction onset temperature was higher for the smaller/rougher Pt nanoparticles than for the smooth Pt surfaces. The rougher surfaces were poisoned by carbon coking, detected by NAP-XPS, and explained by DFT calculations via CO disproportionation on favorable sites. Only after the removal of the carbon deposits did the rough Pt surfaces become active, but at 50 °C higher temperature than for smooth Pt. Upon cooldown, the smooth Pt films exhibited a wider hysteresis window and were hardly affected by CO disproportionation. Future studies of ALD Pt particles and films on different support materials should reveal whether reducible supports facilitate activation at lower temperature and reduce/suppress the initial carbon poisoning.

■ ASSOCIATED CONTENT

Supporting Information

The Supporting Information is available free of charge at https://pubs.acs.org/doi/10.1021/acscatal.0c03974.

Model catalysts; *operando* methods; measurements of CO adsorption and dissociation; DFT calculations; measurements of CO oxidation (PDF)

■ AUTHOR INFORMATION

Corresponding Author

Günther Rupprechter − *Institute of Materials Chemistry, Technische Universität Wien, Vienna 1060, Austria;* orcid.org/0000-0002-8040-1677; Email: guenther.rupprechter@tuwien.ac.at

Authors

Verena Pramhaas − *Institute of Materials Chemistry, Technische Universität Wien, Vienna 1060, Austria*

Matteo Roiaz − *Institute of Materials Chemistry, Technische Universität Wien, Vienna 1060, Austria;* orcid.org/0000-0001-6896-4592

Noemi Bosio − *Department of Physics and Competence Centre for Catalysis, Chalmers University of Technology, Gothenburg 41296, Sweden*

Manuel Corva − *Department of Physics, University of Trieste, 34127 Trieste, Italy; IOM-CNR Laboratorio TASC, 34149 Trieste, Italy*

Christoph Rameshan − *Institute of Materials Chemistry, Technische Universität Wien, Vienna 1060, Austria;* orcid.org/0000-0002-6340-4147

Erik Vesselli − *Department of Physics, University of Trieste, 34127 Trieste, Italy; IOM-CNR Laboratorio TASC, 34149 Trieste, Italy;* orcid.org/0000-0002-6799-0032

Henrik Grönbeck − *Department of Physics and Competence Centre for Catalysis, Chalmers University of Technology, Gothenburg 41296, Sweden;* orcid.org/0000-0002-8709-2889

Complete contact information is available at: https://pubs.acs.org/10.1021/acscatal.0c03974

Author Contributions

SFG measurements were performed by V.P., M.R., M.C., and E.V. and NAP-XPS was conducted by V.P. and C.R. DFT calculations were carried out by N.B and H.G. G.R. acquired funding and coordinated the experimental work. Final interpretation and manuscript preparation were led by V.P. and G.R., with contributions from all authors.

Notes

The authors declare no competing financial interest.

■ ACKNOWLEDGMENTS

G.R. acknowledges funding by the Austrian Science Fund (FWF; projects DK+ Solids4Fun W1243, SFB FOXSI F4502-N16 and Single Atom Catalysis I4434-N) and TU Wien (IP 2008 "SFG Spectroscopy"). H.G. acknowledges financial support from the Swedish Research Council (2016-05234). The calculations were performed at C3SE (Göteborg) through an SNIC grant. We are grateful to Ole Bethge, Emmerich Bertagnolli (ZNMS) and Stefan Löffler (USTEM) of TU Wien for the help with ALD deposition and TEM imaging, respectively. We thank MAX IV for providing beamtime (20180016) and Andrey Shavorskiy (MAX IV), Thomas Haunold, and Raffael Rameshan (both TU Wien) for the assistance.

■ ABBREVIATIONS

ALD, atomic layer deposition; DFT, density functional theory; HOMO, highest occupied molecular orbital; MS, mass spectrometry; NAP-XPS, near-ambient pressure X-ray photoelectron spectroscopy; SFG, sum frequency generation; TEM, transmission electron microscopy; UHV, ultrahigh vacuum

■ REFERENCES

(1) Somorjai, G. A.; Li, Y., *Introduction to surface chemistry and catalysis*; John Wiley & Sons: 2010.

(2) Ertl, G.; Freund, H.-J. Catalysis and Surface Science. *Phys. Today* **1999**, *52*, 32−38.

(3) Carrette, L.; Friedrich, K. A.; Stimming, U. Fuel Cells: Principles, Types, Fuels, and Applications. *ChemPhysChem* **2000**, *1*, 162−193.

(4) Liu, K.; Wang, A.; Zhang, T. Recent Advances in Preferential Oxidation of CO Reaction over Platinum Group Metal Catalysts. *ACS Catal.* **2012**, *2*, 1165−1178.
(5) van Spronsen, M. A.; Frenken, J. W. M.; Groot, I. M. N. Surface science under reaction conditions: CO oxidation on Pt and Pd model catalysts. *Chem. Soc. Rev.* **2017**, *46*, 4347−4374.
(6) Liu, L.; Corma, A. Metal Catalysts for Heterogeneous Catalysis: From Single Atoms to Nanoclusters and Nanoparticles. *Chem. Rev.* **2018**, *118*, 4981−5079.
(7) Wang, A.; Li, J.; Zhang, T. Heterogeneous single-atom catalysis. *Nat. Rev. Chem.* **2018**, *2*, 65−81.
(8) Qiao, B.; Wang, A.; Yang, X.; Allard, L. F.; Jiang, Z.; Cui, Y.; Liu, J.; Li, J.; Zhang, T. Single-atom catalysis of CO oxidation using Pt_1/FeO_x. *Nat. Chem.* **2011**, *3*, 634−641.
(9) Gotterbarm, K.; Späth, F.; Bauer, U.; Bronnbauer, C.; Steinrück, H.-P.; Papp, C. Reactivity of Graphene-Supported Pt Nanocluster Arrays. *ACS Catal.* **2015**, *5*, 2397−2403.
(10) Podda, N.; Corva, M.; Mohamed, F.; Feng, Z.; Dri, C.; Dvorák, F.; Matolin, V.; Comelli, G.; Peressi, M.; Vesselli, E. Experimental and Theoretical Investigation of the Restructuring Process Induced by CO at Near Ambient Pressure: Pt Nanoclusters on Graphene/Ir(111). *ACS Nano* **2017**, *11*, 1041−1053.
(11) Bruix, A.; Lykhach, Y.; Matolínová, I.; Neitzel, A.; Skála, T.; Tsud, N.; Vorokhta, M.; Stetsovych, V.; Ševčíková, K.; Myslivečeka, J.; Fiala, R.; Václavů, M.; Prince, K. C.; Bruyère, S.; Potin, V.; Illas, F.; Matolín, V.; Libuda, J.; Neyman, K. M. Maximum Noble-Metal Efficiency in Catalytic Materials: Atomically Dispersed Surface Platinum. *Angew. Chem., Int. Ed.* **2014**, *53*, 10525−10530.
(12) Jones, J.; Xiong, H.; DeLaRiva, A. T.; Peterson, E. J.; Pham, H.; Challa, S. R.; Qi, G.; Oh, S.; Wiebenga, M. H.; Pereira Hernández, X. I.; Wang, Y.; Datye, A. K. Thermally stable single-atom platinum-on-ceria catalysts via atom trapping. *Science* **2016**, *353*, 150.
(13) Vesselli, E.; Peressi, M., Chapter 8 - Nanoscale Control of Metal Clusters on Templating Supports. In *Studies in Surface Science and Catalysis.*, Fornasiero, P.; Cargnello, M., Eds. *Elsevier*: 2017; Vol. *177*, pp. 285−315.
(14) Liu, J.; Lucci, F. R.; Yang, M.; Lee, S.; Marcinkowski, M. D.; Therrien, A. J.; Williams, C. T.; Sykes, E. C. H.; Flytzani-Stephanopoulos, M. Tackling CO Poisoning with Single-Atom Alloy Catalysts. *J. Am. Chem. Soc.* **2016**, *138*, 6396−6399.
(15) Alayoglu, S.; Nilekar, A. U.; Mavrikakis, M.; Eichhorn, B. Ru-Pt core-shell nanoparticles for preferential oxidation of carbon monoxide in hydrogen. *Nat. Mater.* **2008**, *7*, 333−338.
(16) Campbell, C. T. Ultrathin metal films and particles on oxide surfaces: structural, electronic and chemisorptive properties. *Surf. Sci. Rep.* **1997**, *27*, 1−111.
(17) Vayssilov, G. N.; Lykhach, Y.; Migani, A.; Staudt, T.; Petrova, G. P.; Tsud, N.; Skála, T.; Bruix, A.; Illas, F.; Prince, K. C.; Matolín, V.; Neyman, K. M.; Libuda, J. Support nanostructure boosts oxygen transfer to catalytically active platinum nanoparticles. *Nat. Mater.* **2011**, *10*, 310−315.
(18) Suchorski, Y.; Kozlov, S. M.; Bespalov, I.; Datler, M.; Vogel, D.; Budinska, Z.; Neyman, K. M.; Rupprechter, G. The role of metal/oxide interfaces for long-range metal particle activation during CO oxidation. *Nat. Mater.* **2018**, *17*, 519−522.
(19) Pacchioni, G.; Freund, H.-J. Controlling the charge state of supported nanoparticles in catalysis: lessons from model systems. *Chem. Soc. Rev.* **2018**, *47*, 8474−8502.
(20) Freund, H.-J.; Pacchioni, G. Oxide ultra-thin films on metals: new materials for the design of supported metal catalysts. *Chem. Soc. Rev.* **2008**, *37*, 2224−2242.
(21) An, K.; Alayoglu, S.; Musselwhite, N.; Plamthottam, S.; Melaet, G.; Lindeman, A. E.; Somorjai, G. A. Enhanced CO Oxidation Rates at the Interface of Mesoporous Oxides and Pt Nanoparticles. *J. Am. Chem. Soc.* **2013**, *135*, 16689−16696.
(22) Somorjai, G. A. Surface science at high pressures. *Z. Phys. Chem.* **1996**, *197*, 1−19.
(23) Baldelli, S.; Eppler, A. S.; Anderson, E.; Shen, Y. R.; Somorjai, G. A. Surface enhanced sum frequency generation of carbon monoxide adsorbed on platinum nanoparticle arrays. *J. Chem. Phys.* **2000**, *113*, 5432−5438.
(24) Rupprechter, G.; Dellwig, T.; Unterhalt, H.; Freund, H.-J. CO adsorption on Ni(100) and Pt(111) studied by infrared−visible sum frequency generation spectroscopy: design and application of an SFG-compatible UHV−high-pressure reaction cell | SpringerLink. *Top. Catal.* **2001**, *15*, 19−26.
(25) Freund, H.-J.; Bäumer, M.; Libuda, J.; Risse, T.; Rupprechter, G.; Shaikhutdinov, S. Preparation and characterization of model catalysts: from ultrahigh vacuum to in situ conditions at the atomic dimension. *J. Catal.* **2003**, *216*, 223−235.
(26) Rupprechter, G. Sum Frequency Laser Spectroscopy during Chemical Reactions on Surfaces. *MRS Bull.* **2007**, *32*, 1031−1037.
(27) Rupprechter, G., Sum Frequency Generation and Polarization−Modulation Infrared Reflection Absorption Spectroscopy of Functioning Model Catalysts from Ultrahigh Vacuum to Ambient Pressure. In *Adv. Catal.*, Gates, B. C.; Knözinger, H., Eds. Academic Press: 2007; Vol. *51*, pp. 133−263.
(28) Somorjai, G. A.; York, R. L.; Butcher, D.; Park, J. Y. The evolution of model catalytic systems; studies of structure, bonding and dynamics from single crystal metal surfaces to nanoparticles, and from low pressure ($<10^{-3}$ Torr) to high pressure ($>10^{-3}$ Torr) to liquid interfaces. *Phys. Chem. Chem. Phys.* **2007**, *9*, 3500−3513.
(29) Salmeron, M.; Schlögl, R. Ambient pressure photoelectron spectroscopy: A new tool for surface science and nanotechnology. *Surf. Sci. Rep.* **2008**, *63*, 169−199.
(30) Rupprechter, G.; Weilach, C. Spectroscopic studies of surface-gas interactions and catalyst restructuring at ambient pressure: mind the gap! *J. Phys.: Condens. Matter* **2008**, *20*, 184019.
(31) Gao, F.; Wang, Y.; Cai, Y.; Goodman, D. W. CO Oxidation on Pt-Group Metals from Ultrahigh Vacuum to Near Atmospheric Pressures. 2. Palladium and Platinum. *J. Phys. Chem. C* **2009**, *113*, 174−181.
(32) Jiang, T.; Mowbray, D. J.; Dobrin, S.; Falsig, H.; Hvolbæk, B.; Bligaard, T.; Nørskov, J. K. Trends in CO Oxidation Rates for Metal Nanoparticles and Close-Packed, Stepped, and Kinked Surfaces. *J. Phys. Chem. C* **2009**, *113*, 10548−10553.
(33) Sauer, J.; Freund, H.-J. Models in Catalysis. *Catal. Lett.* **2015**, *145*, 109−125.
(34) Anic, K.; Wolfbeisser, A.; Li, H.; Rameshan, C.; Föttinger, K.; Bernardi, J.; Rupprechter, G. Surface Spectroscopy on UHV-Grown and Technological Ni−ZrO_2 Reforming Catalysts: From UHV to Operando Conditions. *Top. Catal.* **2016**, *59*, 1614−1627.
(35) Hayek, K.; Fuchs, M.; Klötzer, B.; Reichl, W.; Rupprechter, G. Studies of metal−support interactions with "real" and "inverted" model systems: reactions of CO and small hydrocarbons with hydrogen on noble metals in contact with oxides. *Top. Catal.* **2000**, *13*, 55−66.
(36) Palomino, R. M.; Gutiérrez, R. A.; Liu, Z.; Tenney, S.; Grinter, D. C.; Crumlin, E.; Waluyo, I.; Ramírez, P. J.; Rodriguez, J. A.; Senanayake, S. D. Inverse Catalysts for CO Oxidation: Enhanced Oxide−Metal Interactions in MgO/Au(111), CeO_2/Au(111), and TiO_2/Au(111). *ACS Sustainable Chem. Eng.* **2017**, *5*, 10783−10791.
(37) Rameshan, C.; Li, H.; Anic, K.; Roiaz, M.; Pramhaas, V.; Rameshan, R.; Blume, R.; Hävecker, M.; Knudsen, J.; Knop-Gericke, A.; Rupprechter, G. In situ NAP-XPS spectroscopy during methane dry reforming on ZrO_2/Pt(1 1 1) inverse model catalyst. *J. Phys.: Condens. Matter* **2018**, *30*, 264007.
(38) Ritala, M.; Niinistö, J. Industrial Applications of Atomic Layer Deposition. *ECS Trans.* **2009**, *25*, 641−652.
(39) Kääriäinen, T.; Cameron, D.; Kääriäinen, M. L.; Sherman, A., ALD Applications and Industry. In *Atomic Layer Deposition: Principles, Characteristics, and Nanotechnology Applications, Second Edition*, Scrivener Publishing LLC: 2013; pp. 215−242.
(40) Lu, J.; Elam, J. W.; Stair, P. C. Atomic layer deposition—Sequential self-limiting surface reactions for advanced catalyst "bottom-up" synthesis. *Surf. Sci. Rep.* **2016**, *71*, 410−472.

(41) Lee, H.-B.-R.; Mullings, M. N.; Jiang, X.; Clemens, B. M.; Bent, S. F. Nucleation-Controlled Growth of Nanoparticles by Atomic Layer Deposition. *Chem. Mater.* **2012**, *24*, 4051−4059.
(42) ALD NanoSolutions. https://www.aldnanosolutions.com/.
(43) Ding, K.; Gulec, A.; Johnson, A. M.; Schweitzer, N. M.; Stucky, G. D.; Marks, L. D.; Stair, P. C. Identification of active sites in CO oxidation and water-gas shift over supported Pt catalysts. *Science* **2015**, *350*, 189.
(44) Wang, H.-F.; Gan, W.; Lu, R.; Rao, Y.; Wu, B.-H. Quantitative spectral and orientational analysis in surface sum frequency generation vibrational spectroscopy (SFG-VS). *Int. Rev. Phys. Chem.* **2005**, *24*, 191−256.
(45) Lu, R.; Gan, W.; Wu, B.-H.; Chen, H.; Wang, H.-F. Vibrational Polarization Spectroscopy of CH Stretching Modes of the Methylene Group at the Vapor/Liquid Interfaces with Sum Frequency Generation. *J. Phys. Chem. B* **2004**, *108*, 7297−7306.
(46) Galletto, P.; Unterhalt, H.; Rupprechter, G. The molecular orientation of CO on Pd(111): a polarization-dependent SFG study. *Chem. Phys. Lett.* **2003**, *367*, 785−790.
(47) Li, X.; Roiaz, M.; Pramhaas, V.; Rameshan, C.; Rupprechter, G. Polarization-Dependent SFG Spectroscopy of Near Ambient Pressure CO Adsorption on Pt(111) and Pd(111) Revisited. *Top. Catal.* **2018**, *61*, 751−762.
(48) Xu, J.; Yates, J. T., Jr. Terrace width effect on adsorbate vibrations- A comparison of Pt(335) and Pt(112) for chemisorption of CO. *Surf. Sci.* **1995**, *327*, 193−201.
(49) Tüshaus, M.; Schweizer, E.; Hollins, P.; Bradshaw, A. M. Yet another vibrat1onal study of the adsorption system Pt{111}-CO. *J. Electron Spectrosc. Relat. Phenom.* **1987**, *44*, 305−316.
(50) Shen, Y. R. Surface properties probed by second-harmonic and sum-frequency generation. *Nature* **1989**, *337*, 519−525.
(51) Morkel, M.; Unterhalt, H.; Klüner, T.; Rupprechter, G.; Freund, H.-J. Interpreting intensities in vibrational sum frequency generation (SFG) spectroscopy: CO adsorption on Pd surfaces. *Surf. Sci.* **2005**, *586*, 146−156.
(52) Höbel, F.; Bandara, A.; Rupprechter, G.; Freund, H.-J. Deactivation of Pd particles supported on $Nb_2O_5/Cu_3Au(100)$: SFG and TPD studies from UHV to 100mbar. *Surf. Sci.* **2006**, *600*, 963−970.
(53) Rupprechter, G.; Dellwig, T.; Unterhalt, H.; Freund, H.-J. High-Pressure Carbon Monoxide Adsorption on Pt(111) Revisited: A Sum Frequency Generation Study. *J. Phys. Chem. B* **2001**, *105*, 3797−3802.
(54) Hayden, B. E.; Kretzschmar, K.; Bradshaw, A. M.; Greenler, R. G. An infrared study of the adsorption of CO on a stepped platinum surface. *Surf. Sci.* **1985**, *149*, 394−406.
(55) Backus, E. H. G.; Bonn, M. A quantitative comparison between reflection absorption infrared and sum-frequency generation spectroscopy. *Chem. Phys. Lett.* **2005**, *412*, 152−157.
(56) Klünker, C.; Balden, M.; Lehwald, S.; Daum, W. CO stretching vibrations on Pt(111) and Pt(110) studied by sum frequency generation. *Surf. Sci.* **1996**, *360*, 104−111.
(57) Härle, H.; Mendel, K.; Metka, U.; Volpp, H. R.; Willms, L.; Wolfrum, J. Temperature dependence (90−440 K) of the vibrational spectra of CO adsorbed on platinum(111) studied by sum-frequency generation. *Chem. Phys. Lett.* **1997**, *279*, 275−281.
(58) Jørgensen, M.; Grönbeck, H. Scaling Relations and Kinetic Monte Carlo Simulations To Bridge the Materials Gap in Heterogeneous Catalysis. *ACS Catal.* **2017**, *7*, 5054−5061.
(59) Tränkenschuh, B.; Fritsche, N.; Fuhrmann, T.; Papp, C.; Zhu, J. F.; Denecke, R.; Steinrück, H.-P. A site-selective in situ study of CO adsorption and desorption on Pt(355). *J. Chem. Phys.* **2006**, *124*, No. 074712.
(60) McCrea, K.; Parker, J. S.; Chen, P.; Somorjai, G. Surface structure sensitivity of high-pressure CO dissociation on Pt(557), Pt(100) and Pt(111) using sum frequency generation surface vibrational spectroscopy. *Surf. Sci.* **2001**, *494*, 238−250.
(61) Vandichel, M.; Grönbeck, H. A dimer path for CO dissociation on PtSn. *Catal. Sci. Technol.* **2019**, *9*, 695−701.
(62) Olmos-Asar, J. A.; Monachino, E.; Dri, C.; Peronio, A.; Africh, C.; Lacovig, P.; Comelli, G.; Baldereschi, A.; Peressi, M.; Vesselli, E. CO on Supported Cu Nanoclusters: Coverage and Finite Size Contributions to the Formation of Carbide via the Boudouard Process. *ACS Catal.* **2015**, *5*, 2719−2726.
(63) Ng, M. L.; Abild-Pedersen, F.; Kaya, S.; Mbuga, F.; Ogasawara, H.; Nilsson, A. Low Barrier Carbon Induced CO Dissociation on Stepped Cu. *Phys. Rev. Lett.* **2015**, *114*, 246101.
(64) Trinchero, A.; Hellman, A.; Grönbeck, H. Methane oxidation over Pd and Pt studied by DFT and kinetic modeling. *Surf. Sci.* **2013**, *616*, 206−213.
(65) Deutschmann, O.; Schmidt, R.; Behrendt, F.; Warnat, J. Numerical modeling of catalytic ignition. *ymp. (Int.) Combust.* **1996**, *26*, 1747−1754.
(66) Vogel, D.; Spiel, C.; Suchorski, Y.; Trinchero, A.; Schlögl, R.; Grönbeck, H.; Rupprechter, G. Local Catalytic Ignition during CO Oxidation on Low-Index Pt and Pd Surfaces: A Combined PEEM, MS, and DFT Study. *Angew. Chem., Int. Ed.* **2012**, *51*, 10041−10044.
(67) Perez-Alonso, F. J.; McCarthy, D. N.; Nierhoff, A.; Hernandez-Fernandez, P.; Strebel, C.; Stephens, I. E. L.; Nielsen, J. H.; Chorkendorff, I. The Effect of Size on the Oxygen Electroreduction Activity of Mass-Selected Platinum Nanoparticles. *Angew. Chem., Int. Ed.* **2012**, *51*, 4641−4643.
(68) Jørgensen, M.; Grönbeck, H. The Site-Assembly Determines Catalytic Activity of Nanoparticles. *Angew. Chem., Int. Ed.* **2018**, *57*, 5086−5089.
(69) Pazhetnov, E. M.; Koshcheev, S. V.; Boronin, A. I. Formation Mechanism and Structure of Monatomic Carbon Films in Ethylene Decomposition on the Pt(111) Surface According to XPS Data. *Kinet. Catal.* **2003**, *44*, 414−419.
(70) Toyoshima, R.; Yoshida, M.; Monya, Y.; Suzuki, K.; Amemiya, K.; Mase, K.; Mun, B. S.; Kondoh, H. A high-pressure-induced dense CO overlayer on a Pt (111) surface: a chemical analysis using in situ near ambient pressure XPS. *Phys. Chem. Chem. Phys.* **2014**, *16*, 23564−23567.

https://dx.doi.org/10.1021/acscatal.0c03974
ACS Catal. 2021, 11, 208−214